Check for updates

ADVANCED FUNCTIONAL MATERIALS
www.afm-journal.de

The Electrode-Ferroelectric Interface as the Primary Constraint on Endurance and Retention in HZO-Based Ferroelectric Capacitors

Ruben Alcala, Monica Materano, Patrick D. Lomenzo, Pramoda Vishnumurthy, Wassim Hamouda, Catherine Dubourdieu, Alfred Kersch, Nicolas Barrett, Thomas Mikolajick, and Uwe Schroeder**

Ferroelectric hafnium-zirconium oxide is one of the most relevant CMOS-compatible materials for next-generation, non-volatile memory devices. Nevertheless, performance reliability remains an issue. With TiN electrodes (the most reported electrode material), Hf-Zr-based ferroelectric capacitors struggle to provide reliable retention due to electrode-ferroelectric interface interactions. Although Hf-Zr-based ferroelectric capacitors are fabricated with other electrodes, the focus is predominantly directed toward obtaining a large ferroelectric response. The impact of the electrodes on data retention for these ferroelectrics remains underreported and greater insight is needed to improve device reliability. Here, a comprehensive set of electrodes are evaluated with emphasis on the core ferroelectric memory reliability metrics of endurance, retention, and imprint. Metal-ferroelectric-metal capacitors comprised of a $Hf_{0.5}Zr_{0.5}O_2$ layer deposited between different combinations of nitride (TiN, TiAlN, and NbN), pure metal (W), and oxide (MoO_2, RuO_2, and IrO_2) top and bottom electrodes are fabricated for the investigation. From the electrical, physical, and structural analysis, the low reactivity of the electrode with the ferroelectric is found to be key for improved reliability of the ferroelectric capacitor. This understanding of interface properties provides necessary insight for the broad implementation of Hf-Zr-based ferroelectrics in memory technology and, overall, boosts the development of next-generation memories.

1. Introduction

Hafnium-zirconium oxide (HZO) is very appealing for complementary metal–oxid–esemiconductor (CMOS)-compatible non-volatile ferroelectric memory applications. Nevertheless, reliability remains an issue.[1,2] Due to the roughly 5–15 nm film thickness range of interest for memory applications, the electrode-ferroelectric interface arguably plays a more important role than for thicker perovskite ferroelectrics. Consequently, different electrode materials have been studied.[3,5] TiN electrodes are by far the most commonly reported electrode material for HZO-based ferroelectric capacitors (FeCaps).[6] That said, other examples include similar metal nitride electrodes, like TaN,[7,8] pure metals, like W, Pt, Ru, and Ir,[9,12] and metal oxides, like IrO_2 and RuO_2.[13,17] These former reports show that the electrode-ferroelectric interface plays a key role in defining the ferroelectric response of the FeCap, but most only evaluated a couple of electrode materials at a time. Due to the varying film fabrication conditions in

R. Alcala, M. Materano, P. D. Lomenzo, P. Vishnumurthy, T. Mikolajick, U. Schroeder
NaMLab gGmbH
Noethnitzer Strasse 64a, 01187 Dresden, Germany
E-mail: ruben.alcala@mailbox.tu-dresden.de; uwe.schroeder@namlab.com

R. Alcala, T. Mikolajick
TU Dresden
Chair of Nanoelectronics
Noethnitzer Strasse 64, 01187 Dresden, Germany

W. Hamouda, C. Dubourdieu
Helmholtz-Zentrum Berlin für Materialien und Energie
Insitute Functional Oxides for Energy-Efficient Information Technology
Hahn-Meitner Platz 1, 14109 Berlin, Germany

W. Hamouda, N. Barrett
SPEC
CEA
CNRS
Universite Paris-Saclay
CEA Saclay
Gif-sur-Yvette 91191, France

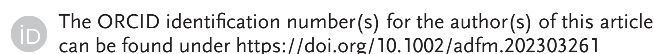
The ORCID identification number(s) for the author(s) of this article can be found under https://doi.org/10.1002/adfm.202303261

© 2023 The Authors. Advanced Functional Materials published by Wiley-VCH GmbH. This is an open access article under the terms of the Creative Commons Attribution-NonCommercial-NoDerivs License, which permits use and distribution in any medium, provided the original work is properly cited, the use is non-commercial and no modifications or adaptations are made.

DOI: 10.1002/adfm.202303261

previous works, it is difficult to distinguish the impact of the electrodes from other effects clearly. Thus, an investigation of electrode materials with otherwise identical ferroelectric film processing provides more precise insights into FeCap reliability.

From the work on doped HfO_2 with TaN electrodes,[7,8] the tendency of the top and bottom electrode to asymmetrically oxidize to create an oxide interface layer with HfO_2 agrees with what has been observed for TiN.[4] An increase in oxygen vacancies (V_O) generated by TaN, compared to TiN, can improve remanent polarization (P_r) in one orientation but worsens the field cycling endurance of the device.[18]

In the work of Park et al. on $Hf_{0.5}Zr_{0.5}O_2$ (HZO),[9] a comparison between the standard TiN and Pt bottom electrode (BE) is discussed. According to their study, TiN bottom electrodes (BEs) promote high tensile stress along the c-axis of the stabilized tetragonal phase (*t*-phase), enhancing ferroelectricity. A similar finding is reported by Cao et al.,[3] who employed Pt, along with Pd, Au, W, Al, and Ta, as the top electrode (TE), and kept TiN as the bottom electrode. Different thermal expansion coefficient mismatches were measured between HfO_2 and the electrode material, causing a different stress in the ferroelectric layer. W yielded the highest remanent polarization among the TE materials, followed by TiN and Pt ($2P_r$ = 36.9, 38.7, and 32.7 μC cm^{-1},[2] respectively).

W seemed advantageous not only because of stress-tuning but also because of the suppression of the formation of an oxide interface layer between the BE and the ferroelectric layer. The latter is most likely formed at the beginning of the HfO_2 deposition process or because of exposure of the BE to the atmosphere between the different processing steps.[4] Lee et al.[5] compared W, Ni, TiN, and Mo. Capacitor stacks with a W BE showed limited oxidized interface layer formation and the best ferroelectric properties. Similar findings were reported by Karbasian et al.,[10] where W demonstrated superior properties compared to TiN.

In the work of Park et al.,[11] an IrO_2 interface was formed after depositing the Ir as a bottom electrode due to exposure to the atmosphere between the electrode and the ferroelectric oxide deposition. According to their hypothesis, this interface was then reduced by the HZO, which promoted the stabilization of the non-ferroelectric monoclinic phase (*m*-phase) and the consequent deterioration of the ferroelectric properties because of the accelerated growth and size of the HZO grains during atomic layer deposition (ALD). The polar orthorhombic phase (*o*-phase) was only successfully stabilized for small HZO film thicknesses. Elemental Ru showed low reactivity with HZO, resulting in better performance for Ru/HZO/Ru capacitors compared to TiN/HZO/TiN in terms of leakage current and field cycling endurance.[12]

Former research on $PbZr_xTi_{1-x}O_3$ based devices has shown that metal oxide electrodes seem to be advantageous due to their suppression of oxygen vacancies.[19,20] Nevertheless, mixed results have been reported for HZO-based FeCaps. Mittmann et al.[13] deposited symmetrical HZO-based FeCaps, with IrO_2 as both the TE and BE, and observed a reduction in oxygen vacancies and ferroelectric response. The additional oxygen provided by the oxide electrode seemed to destabilize the polar *o*-phase in favor of the non-polar *m*-phase. An analogous behavior was observed by Park et al.[14] with RuO_2, in addition to reduced endurance. On the other hand, Goh et al.[15,16] have reported a reduced wake-up effect, and improved endurance and retention properties when replacing TiN with RuO_2. These results were attributed to a lack of interfacial oxide layer formation and higher residual tensile stress and were supported by X-ray photoelectron spectroscopy (XPS) measurements.

In summary, the body of evidence makes it clear that the material interactions of the electrode with the FE HZO layer during fabrication and operation can significantly alter the structure and composition of the FeCap. These are primarily the formation of oxide interface layers and stress/strain contributions.[9] In effect, the generated irregularities, such as crystalline defects or oxygen vacancies, that come with these interactions introduce trap sites and mobile charges from an electronic perspective and will contribute to the degradation or breakdown of the device during operation.[21,22] **Figure 1** illustrates a schematic ferroelectric capacitor at zero bias, with such additional contributions introduced into the system and considering a non-ideal electrode with a non-zero charge screening length.

Here, a comprehensive reliability investigation of electrode materials on HZO-based capacitors with nitride, oxide, and elemental metal electrodes is undertaken. The interplay between defects, the electrode interfaces, and the resulting crystalline structure of the HZO films is discussed. In contrast to former studies, an overall reliability comparison where chemical interface properties and defect content can be directly related to field cycling endurance, polarization retention, and especially imprint is presented. The results provide novel insights to engineer the reliability of HZO-based FeCaps by controlling the formation of interface layers and oxygen vacancies.

2. Results and Discussion

2.1. TiN Reference

To establish a baseline with the most commonly reported TiN electrode material, a detailed characterization of the TiN/HZO/TiN capacitor stack is performed as a reference for the stacks containing other electrodes (see Supporting Information for details). Even when the same top and bottom electrode material is used, an asymmetry in the stack is present. As previously reported, the top and bottom electrodes can be oxidized differently depending on the fabrication process sequence.[4,23,24] The TiN BE interface is more likely to form a complete TiO_2 layer before HZO deposition as a result of the exposure to the atmosphere and an oxygen-rich environment in the ALD chamber during the first cycles of the ALD HZO deposition.

The TiN TE, in contrast, is directly deposited on the HZO. Because of this, although the Ti in both electrodes tends to scavenge oxygen from the HZO layer during the annealing to induce crystallization of the HZO layer, the presence of TiO_2 at the bottom interface significantly decreases this effect. Consequently, two

C. Dubourdieu
Freie Universität Berlin
Physical Chemistry
Arnimallee 22, 14195 Berlin, Germany
A. Kersch
University Applied Sciences
Department of Applied Sciences and Mechatronics
Lothstr. 34, 80335 München, Germany

© 2023 The Authors. Advanced Functional Materials published by Wiley-VCH GmbH

16163028, 2023, 43, Downloaded from https://onlinelibrary.wiley.com/doi/10.1002/adfm.202303261 by Freie Universitaet Berlin, Wiley Online Library on [24/10/2023]. See the Terms and Conditions (https://onlinelibrary.wiley.com/terms-and-conditions) on Wiley Online Library for rules of use; OA articles are governed by the applicable Creative Commons License

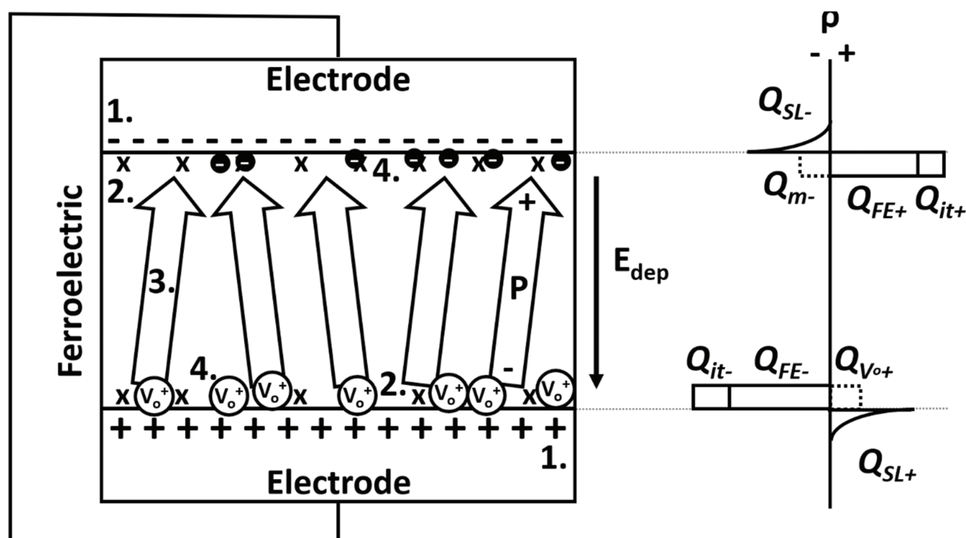

Figure 1. FeCap schematic depicting different charges present in the device under zero external bias but with a fully poled ferroelectric layer and a corresponding charge density plot. 1) Electrode screening charge with a corresponding charge distribution (**+/−**: Q_{SL}), 2) interface trapped charge (**x**: Q_{it}), 3) ferroelectric dipole in an up-state (↑**P**: Q_{FE}), and 4. positive (oxygen vacancies, $\boldsymbol{V_O}$: Q_{Vo}) and negative (●: Q_m) mobile charge.

different TiO_xN_y layers (one at the top and the other at the bottom HZO-TiN interface) are observed with a higher V_O concentration in HZO at the top electrode (0.6%) compared to the bottom electrode case (0.15%).[4] From an electronic energy level perspective, the different oxidized layers will introduce distinct trap levels, and therefore dissimilar charge distributions. In effect, it is possible for an internal field to arise due to a difference in charge (particularly V_O) at each interface (as shown in Figure 1). Further discussion on oxide formation energies and V_O formation can be found in Supporting Information.

Field cycling endurance and polarization have already been well documented in HZO with TiN electrodes.[25] To better understand field cycling degradation and imprint shift, impedance spectroscopy was implemented in this work during reliability measurements. Impedance was measured after a given number of field cycles or time intervals, and the results were fitted to a two resistor/capacitor (RC)-element analysis model (as shown in **Figure 2** and described elsewhere[26,27]). Starting from pristine interface and bulk resistance values of about 1 kΩ and 500 MΩ, respectively, it was possible to determine a decrease in the interface resistance of roughly 30% and 10% for retention and electric field cycling measurements, respectively. Despite the similar behavior, different causes are expected to be behind each degradation.

For field cycling measurements, an initial drop in interface resistance acts as a first indication for the eventual breakdown of the device, signaling an interface-driven breakdown mechanism. This suggests that the interface may act as a source of defects which then spread throughout the film, creating

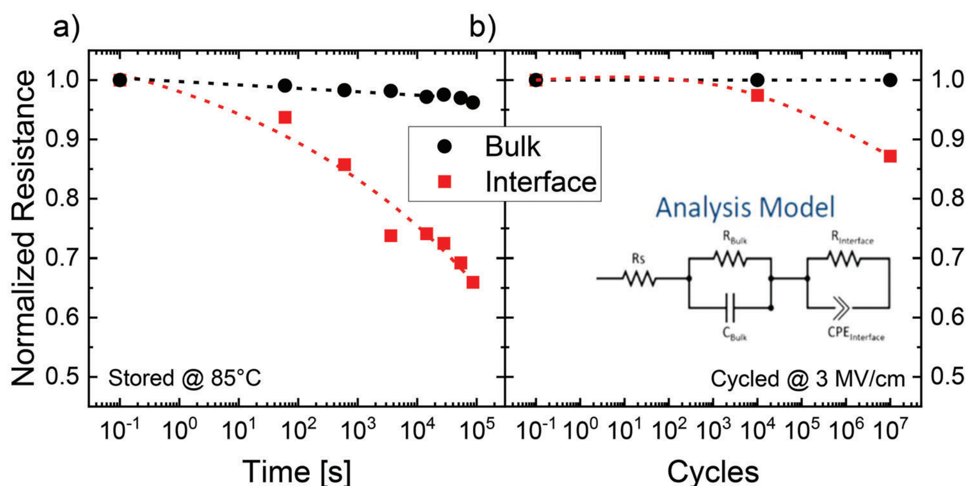

Figure 2. Electrical resistance extracted from an analysis of a two RC-element model fit of an impedance measurement performed on a ferroelectric capacitor with a 10 nm HZO film and TiN TE and BE. The resistance of the RC elements is plotted for a) retention at 85 °C and b) field cycling at 3 MV cm^{-1} (100 kHz). One of the capacitive elements of the analysis model was replaced by a constant phase element (CPE) representing a non-ideal capacitive behavior. For both cases, the capacitor was woken-up up to 10^4 cycles at 3 MV cm^{-1}.

© 2023 The Authors. Advanced Functional Materials published by Wiley-VCH GmbH

16163028, 2023, 43, Downloaded from https://onlinelibrary.wiley.com/doi/10.1002/adfm.202303261 by Freie Universitaet Berlin, Wiley Online Library on [24/10/2023]. See the Terms and Conditions (https://onlinelibrary.wiley.com/terms-and-conditions) on Wiley Online Library for rules of use; OA articles are governed by the applicable Creative Commons License

16163028, 2023, 43, Downloaded from https://onlinelibrary.wiley.com/doi/10.1002/adfm.202303261 by Freie Universitaet Berlin, Wiley Online Library on [24/10/2023]. See the Terms and Conditions (https://onlinelibrary.wiley.com/terms-and-conditions) on Wiley Online Library for rules of use; OA articles are governed by the applicable Creative Commons License

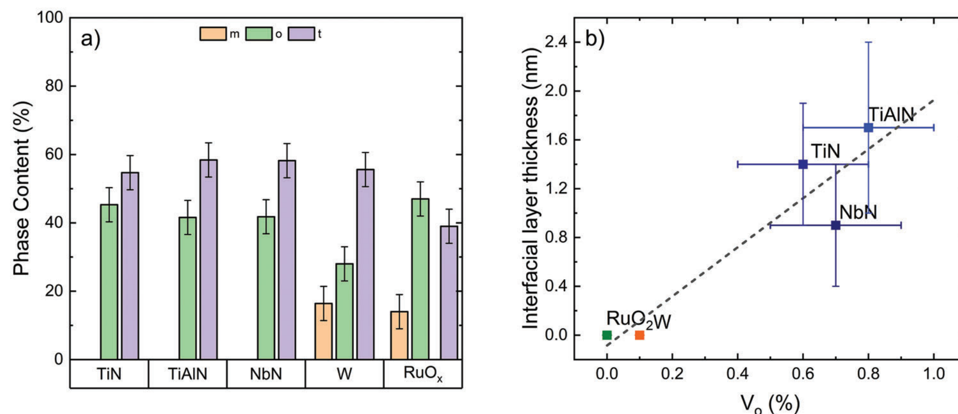

Figure 3. a) Phase content of HZO for capacitor stacks with a TiN BE and different TEs (TiN, TiAlN, NbN, W, and RuO_2). b) Interface layer thickness of the TE as a function of *V*o content in HZO for different TEs as determined by XPS (see Supporting Information).

percolation paths,[28] eventually resulting in the breakdown of the device.[29,30] In contrast, the decrease in resistance observed for the retention measurement matches well with the expected displacement of mobile defect charge toward the interface.[25] It is worth pointing out that, for the interface RC-element of the analysis model, the C element was replaced by a non-ideal capacitive element (i.e., constant-phase-element or CPE) for a better quality fit of the data, suggesting a partially conductive behavior right from the start.

The impedance spectroscopy analysis of the reference TiN/HZO/TiN capacitor stack shows how the interface plays an essential role in device reliability, as it provides the source of V_O that limits retention due to a large imprint. The degradation of the interface also appears to be the first step of the breakdown process during field cycling.

2.2. Top Electrode Comparison

Five different top electrodes were deposited on the same TiN BE/10 nm HZO stack and annealed in N_2 at 600 °C for 20 s. The electrode materials can be separated into three groups: nitrides (TiN, TiAlN, NbN), oxides (MoO_2, RuO_2), and elemental metal (W). The same structural and electrical characterization techniques were performed on the samples as in the previous section. Detailed measurement results can be found in Supporting Information.

First, structural characterization by grazing incidence X-ray diffraction (GIXRD) revealed similarities within each electrode material group after deconvolution of the XRD pattern. As previously discussed for TiN, all nitride top electrodes presented a *t*-phase content in the 50%–65% range, an *o*-phase content of 35%–50%, and a negligible *m*-phase (**Figure 3**a). In contrast, W as a TE resulted in a roughly 25% *o*-phase, 50% *t*-phase, and a 15% *m*-phase content. For oxide electrodes, the *m*-phase content was also close to 15%, *o*-phase was around 45% and *t*-phase about 40% (see Supporting Information for individual fittings). Next, interface layer thickness and V_O were calculated from the fitting of the XPS spectra of Hf *4f* and the corresponding metal of the given electrode (see Supporting Information). From Figure 3b, a direct relation between V_O and interfacial layer thickness is identified, where an interface layer thickness of 0.9 to 1.7 nm for nitride electrodes corresponded to a high V_O content of 0.6%–0.8%, and the remaining electrode materials presented no detectable interface layer formation and a V_O content of 0.1% or lower. From these two analyses, it appears that a higher V_O concentration in the HZO layer, as a result of the electrode oxidizing and forming an interfacial layer, leads to a lower the *m*-phase content. This agrees with previous experimental and simulation findings,[31] where the oxygen content in the HZO layer had a significant impact on the phase composition of the HZO.

Following Ostwald's rule,[32] grain growth during HZO layer crystallization starts via small crystallites in the *t*-phase and, depending on the oxygen content, the activation barrier for a transition to either the *o*- or *m*-phase is more significantly reduced;[31] hence, a preferential phase stabilization. By considering this and comparing oxide formation energies of the different electrode materials (see Supporting Information), it is identified that: the oxide formation energy defines the formation of an interfacial layer, subsequently influencing V_O, and, ultimately, impacting the phase composition of the HZO layer. Thus, despite all samples having the same TiN bottom electrode, the oxygen scavenging of the top electrode strongly impacts the phase formation within the HZO layer.

It is important to consider that the formation of an interfacial layer may reach a non-negligible thickness with respect to the thickness of the ferroelectric, implying an additional dielectric dead layer in the structure.[4] This additional interfacial layer may consequently contribute with a parasitic dielectric dipole which can be further detrimental to reliability performance, particularly in the case of nitride electrodes. Moreover, this additional dielectric lowers the effective electric field across HZO for a nominal applied bias.

Field cycling endurance measurements were performed on all samples (see **Figure 4**). Almost all samples show a field induced *t-o* phase transition, which dominates wake-up.[1] A lower P_r was observed for TiAlN TE, which may be associated with a much larger *t*-phase content than the other TE materials. The only true exception is W as a TE. As can be seen in Figure 4, W TE presented the lowest P_r, reduced endurance, and limited wake-up. The limited P_r and lack of significant wake-up is likely related to a higher *m*-phase content in the HZO. More importantly, the

© 2023 The Authors. Advanced Functional Materials published by Wiley-VCH GmbH

16163028, 2023, 43, Downloaded from https://onlinelibrary.wiley.com/doi/10.1002/adfm.202303261 by Freie Universitaet Berlin, Wiley Online Library on [24/10/2023]. See the Terms and Conditions (https://onlinelibrary.wiley.com/terms-and-conditions) on Wiley Online Library for rules of use; OA articles are governed by the applicable Creative Commons License

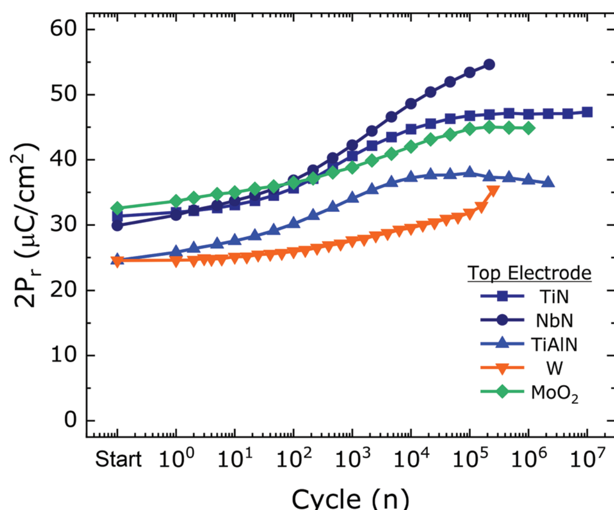

Figure 4. Remanent polarization as a function of number of cycles during field cycling at 3 MV cm^{-1} for nitride, oxide, and W top electrodes where measurements were performed until breakdown of the device except for TiN which was stopped at 10^7 cycles.

expected thin top interfacial oxide layer may be responsible for the reduced endurance. Impedance spectroscopy identified no contribution from an interface layer (see Figure S15, Supporting Information). Therefore, it can be assumed that the formed WO_x layer is conducting and no interface breakdown occurs, as discussed for the TiN in the previous section. Instead, based on models for resistive switching,[33,34] the WO_x layer may further oxidize through cycling, increasing the V_O concentration in the HZO layer, creating percolation paths through the film and, eventually, resulting in the breakdown of the FeCap (see Supporting Information for further discussion).[30]

From **Figure 5**, a higher remanent polarization, as a result of a higher *o*-phase content, is correlated with a reduction of electric field cycling endurance. Pesic et al. showed that a higher $2P_r$ enhances the field during charge injection into the HZO layer during polarization reversal, generating further defects that can lead to earlier breakdown.[1] This general trend could be verified for all electrode materials, with MoO_2 as TE and the nitride electrodes exhibiting higher resilience. The reasons behind the lower than expected endurance of the W TE device may be attributable to enhanced vacancy creation during cycling. The endurance with RuO_2 TE, is below the trend line for its P_r and exhibited a substantial pristine leakage current density, suggesting a possible alternative leakage current and breakdown mechanism.

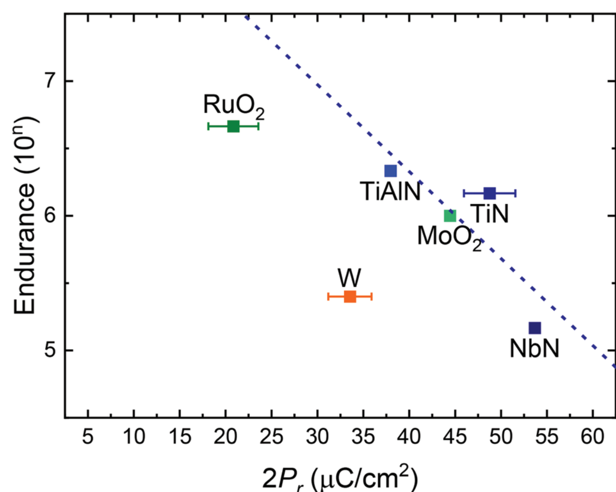

Figure 5. Electric field cycling endurance dependence on a) the woken-up $2P_r$ and b) leakage current density at 3 V in the pristine state. Both curves are for HZO-based ferroelectric capacitors with a TiN BE and different TE materials.

Now, conduction into the HZO layer is compared for the different electrodes. Leakage current measurements[28] before field cycling versus electric field cycling endurance of the different TEs are summarized in **Figure 6**a, with the main trend being a lower endurance for a higher initial leakage current. In Figure 6b, HZO bulk trap distances were calculated from the leakage current measurements, assuming a multi-phonon trap-assisted tunneling model (MPTT).[28] It can be observed how the leakage current increases (right-shift), even after a minor trap distance reduction, after 10[5] cycles, showing signs of degradation in the layer. Last, valence band offsets (VBOs) and conduction band offsets (CBOs) were determined from XPS analysis and plotted as a function of leakage current density in Figure 6c. Despite previously reported differences in work function (WF) for the different TE materials,[35] no simple relation between the CBO and leakage current was observed, within experimental uncertainty. This is to be expected for a bulk trap mediated leakage mechanism, corroborating the multi-phonon trap-assisted tunneling model, which does not depend on charge injection into the conduction band. The only exception to these observations is RuO_2.

All nitride electrodes and W behaved similarly, where an increase in leakage current after cycling was a sign of degradation and a higher leakage current was indicative of lower endurance. Furthermore, the lack of correlation to the calculated CBOs supports a MPTT conduction model. Considering the formation of an interfacial layer during cycling for W, it appears that the presence of an interfacial layer results in a similar band alignment for the discussed electrodes. Hence the similarities in conduction through the HZO layer. Since RuO_2 lacks an interfacial layer formation, it is logical that the larger CBO in Figure 6c matches an expected larger WF (see Supporting Information for calculation).[35] Moreover, a different band alignment would be expected. Therefore a different conduction mechanism may be possible, which explains the lack of correlation of RuO_2 to the trends in Figures 6a,b.

Polarization retention at 85 °C is now discussed, considering imprint as the main limiting factor.[25,36] Imprint was analyzed for each of the capacitor stacks and summarized in **Figure 7** (for details see Supporting Information). A more substantial initial hysteresis shift leads to a more significant imprint slope in one direction. This initial shift may not simply be associated with a WF difference between electrodes, due to Fermi level pinning,[37] but instead also associated with a difference in charge of surface states at each interface. Comparing now the slopes of the imprint measurements for each electrode, it is clear from Figure 7a that, regardless of the TEs, imprint depends primarily on P_r. A large P_r presents a stronger internal field, enhancing the drift of oxygen

 © 2023 The Authors. Advanced Functional Materials published by Wiley-VCH GmbH

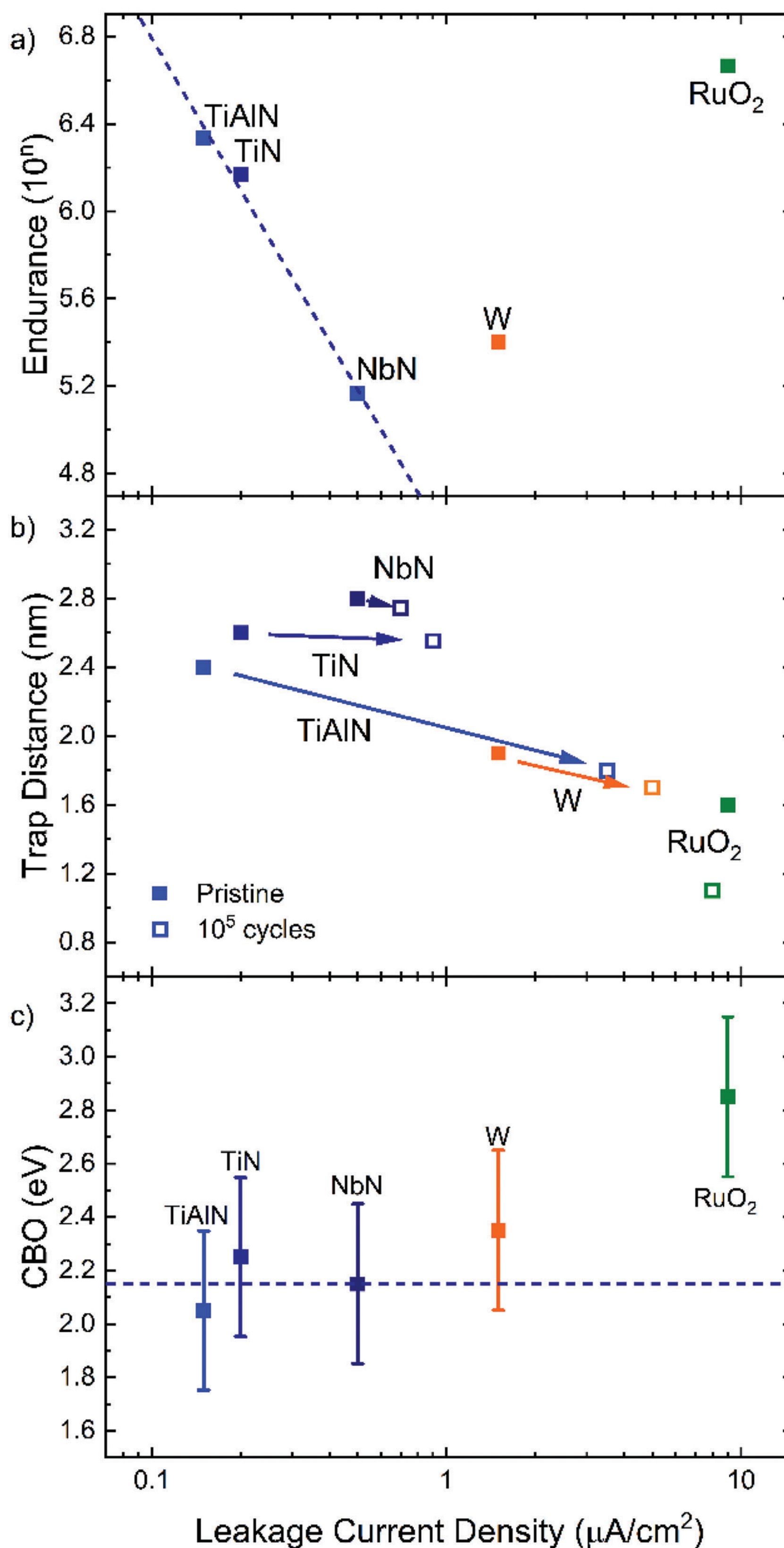

Figure 6. a) Endurance, b) trap distance, and c) onduction band offset (CBO) versus leakage current density at 3 MV cm^{-1} in the pristine state and, for b), after 10^5 cycles. All data points correspond to HZO-based ferroelectric capacitors with a TiN BE and different TE materials.

© 2023 The Authors. Advanced Functional Materials published by Wiley-VCH GmbH

16163028, 2023, 43, Downloaded from https://onlinelibrary.wiley.com/doi/10.1002/adfm.202303261 by Freie Universitaet Berlin, Wiley Online Library on [24/10/2023]. See the Terms and Conditions (https://onlinelibrary.wiley.com/terms-and-conditions) on Wiley Online Library for rules of use; OA articles are governed by the applicable Creative Commons License

16163028, 2023, 43, Downloaded from https://onlinelibrary.wiley.com/doi/10.1002/adfm.202303261 by Freie Universitaet Berlin, Wiley Online Library on [24/10/2023]. See the Terms and Conditions (https://onlinelibrary.wiley.com/terms-and-conditions) on Wiley Online Library for rules of use; OA articles are governed by the applicable Creative Commons License

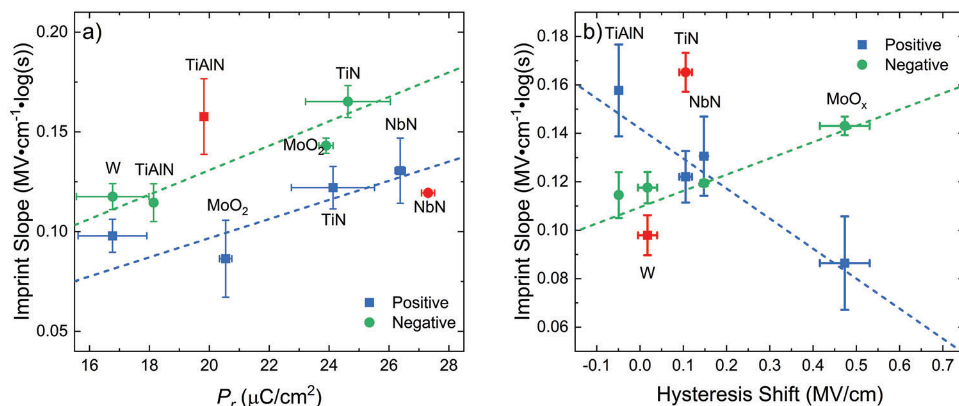

Figure 7. Imprint slope (rate of change in imprint) versus a) remanent polarization and b) hysteresis shift for $Hf_{0.5}Zr_{0.5}O_2$ -based ferroelectric capacitor with a TiN BE and different TE materials. Capacitors were measured after a wake-up cycling of 10^4 cycles.

vacancies within the ferroelectric material. For Figure 7b, the limited measurement voltage range must also be considered. That is, for a limited voltage range (±3 V for this case) and an initial hysteresis shift, imprint will saturate faster in the direction of the initial hysteresis shift and, consequently, will saturate slower in the opposite direction.

In addition to P_r, if one compares the imprint slope to the respective V_O, shown in **Figure 8**, one can observe how a higher V_O leads to a stronger imprint. A higher V_O concentration may provide a steeper V_O profile and, therefore, more significant imprint.

It is clear that the crystalline phase, the symmetry of the ferroelectric hysteresis, the behavior with respect to field cycling, and polarization retention all depend on the formation of a parasitic interface between the electrode material and the ferroelectric oxide. Moreover, a further reaction with the HZO layer during device operation, particularly W oxidation during field cycling, can be detrimental to performance. Interface properties are of fundamental importance because they govern the oxygen exchange between the hafnia layer and the electrode itself, influencing layer

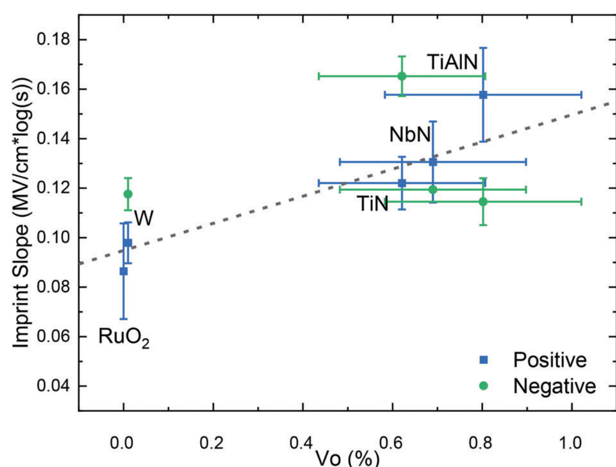

Figure 8. The positive imprint slope (rate of change in imprint) versus V_O for $Hf_{0.5}Zr_{0.5}O_2$-based ferroelectric capacitor with a TiN BE and different TE materials. Capacitors measured after wake-up cycling of 10^4 cycles.

defectivity, that is, the concentration and distribution of V_O in the ferroelectric layer. A variation in the V_O content affects both crystallization behavior and reliability because of defect redistribution.

2.3. Bottom Electrode Comparison

The measurements in the previous section showed a trend in oxidation among the different electrode classes (from oxides to nitrides and metals). For the sake of brevity, only one representative electrode was chosen for each category: TiN (nitride), MoO_2 (oxide), and W (metal). Therefore, three different BEs on a capacitor stack with a TiN top electrode are now introduced into the discussion.

First, the GIXRD analysis (**Figure 9**a) shows a similar trend to that for the TE. An HZO layer on a TiN bottom electrode is crystallized in a 45% *o*-phase and 55% *t*-phase mixture. A W bottom electrode resulted in a high *o*-phase content of 55% with a m- and *t*-phase content 10 and 35%. MoO_2 had a similar *o*-phase content and a *m*- and *t*-phase content of about 20%. Despite other factors potentially influencing P_r for different electrode configurations, such as differences in interface layer formation and V_O concentration, a linear trend within a ±5% error margin is found when plotting the *o*-phase content as a function of remanent polarization for all cases (Figure 9b). Furthermore, modifying the BE from TiN consistently increased P_r, with the opposite being true for the TE. For TiN, an orientational alignment of HZO to the BE is shown in TEM measurements.[38] Song et al. reported for epitaxial growth of HZO on different strained LSMO BE layers that a higher tensile stress of the LSMO film on the HZO film led to increased remanent polarization.[39] As a simple approximation, in **Figure 10**, $2P_r$ versus HZO/BE is plotted for each lattice parameter of the BE as taken from literature.[40] In general, an increased $2P_r$ value for a higher HZO/electrode lattice parameter ratio is visible, which can be related to a higher tensile stress/strain in the layer. MoO_2 has lattice parameters close to HZO and the highest $2P_r$ values. All other electrodes have lower lattice parameters and accordingly lower $2P_r$. Hence, trends determined for epitaxial layers can also be observed for polycrystalline films. Furthermore, assuming local interfacial alignment,

© 2023 The Authors. Advanced Functional Materials published by Wiley-VCH GmbH

16163028, 2023, 43, Downloaded from https://onlinelibrary.wiley.com/doi/10.1002/adfm.202303261 by Freie Universitaet Berlin, Wiley Online Library on [24/10/2023]. See the Terms and Conditions (https://onlinelibrary.wiley.com/terms-and-conditions) on Wiley Online Library for rules of use; OA articles are governed by the applicable Creative Commons License

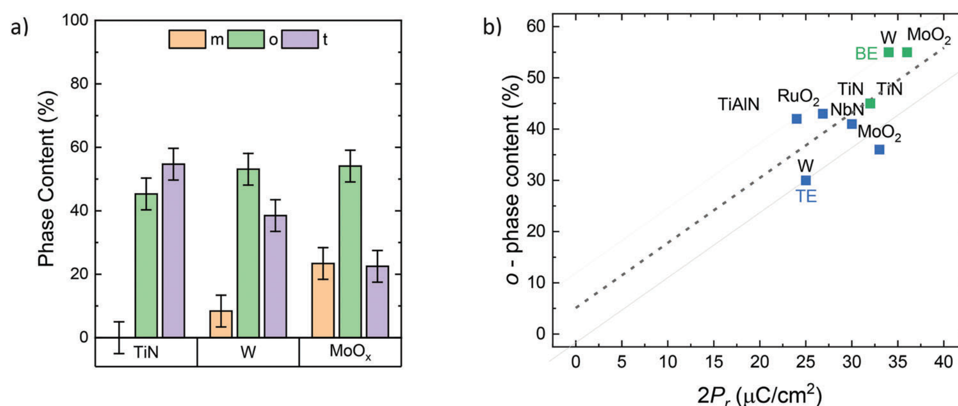

Figure 9. a) Phase composition for HZO capacitors with TiN TE and different BE materials. b) o-phase content as a function of remanent polarization for HZO capacitors with TiN TE (blue symbols) and different bottom electrode materials in contrast to TiN BE (green symbols) with different TE materials.

oxygen content in HZO and interface stress are the crucial parameters influencing the phase formation.

As shown in **Table 1**, V_O concentrations at the BE/HZO interface are much lower compared to the case where the TE interface is modified: 0.15% for TiN/HZO and 0.3% for W/HZO. Unfortunately, no MoO_2 bottom electrode was available for hard x–ray photoelectron spectroscopy (HAXPES) measurements, but similar results for the IrO_2/HZO interface revealed no V_O within the measurement limit, as expected for oxide electrodes.[42] The main difference between an electrode material as a top or bottom electrode is that the HZO layer is deposited atop the bottom electrode. This implies an exposition of the BE to the oxygen ALD precursor, which can, in some cases, oxidize the bottom electrode. This pre-HZO oxide interface layer can act as a diffusion barrier against further oxygen scavenging from the HZO.[23] In addition, from a rough estimation of the BE work function determined from the shift of the polarization hysteresis, similar values to TiN of 4.5 to 4.8 eV were observed (see Supporting Information for calculation), suggesting a comparable band alignment (Table 1).

Table 1. V_O content, interfacial layer thickness, and work function values for different BE.

Bottom electrode	TiN	W	MoO_2
V_O [%]	0.15 ± 0.2	0.3 ± 0.2	–
Interfacial layer thickness [nm]	3.2 ± 0.5	2.5 ± 0.5	–
Work Function [eV]	4.8	4.5	4.8

Next, the impact of the BE on field cycling endurance and breakdown is characterized (**Figure 11**). High $2P_r$ values ranging from 38 to 48 μC cm^{-2} were found for all three cases. Nevertheless, wake-up and fatigue behavior varied. This can be attributed to the difference in crystalline phase content discussed in Figure 9a, as well as to the difference in oxidation for each of the electrodes, creating different interface layers. Nevertheless,

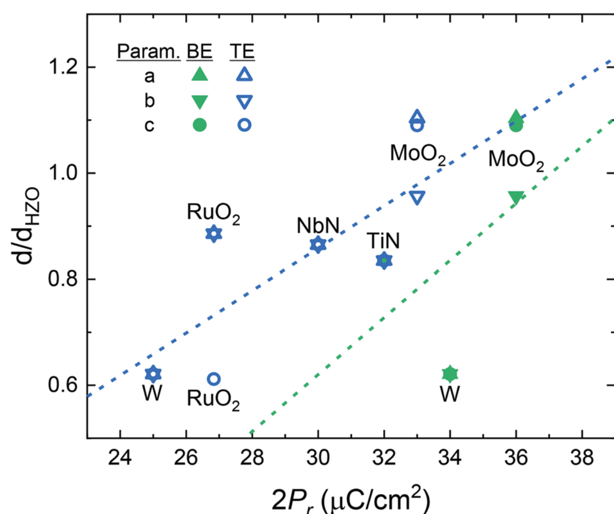

Figure 10. BE/HZO and TE/HZO lattice parameter ratios as a function of remanent polarization. Each of the three lattice parameters (a, b, and c) are compared to HZO, taking all values from the literature.[41] A star-like symbol is a result of overlapping points.

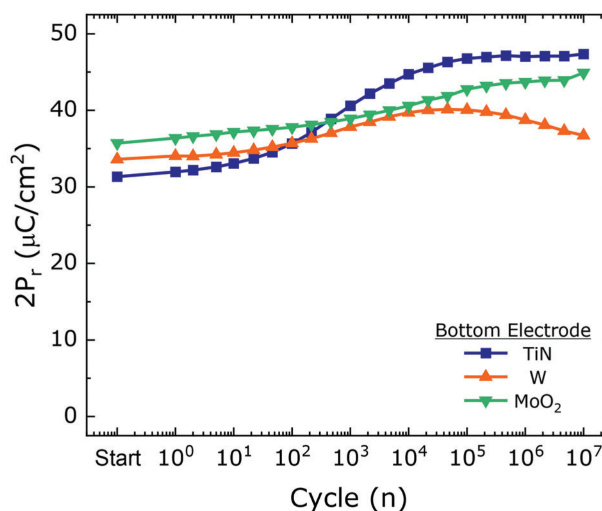

Figure 11. Remanent polarization as a function of field cycling at 3 MV cm^{-1} for HZO capacitors with TiN TE and TiN, W and MoO_2 BE. No breakdown of any device occurred.

© 2023 The Authors. Advanced Functional Materials published by Wiley-VCH GmbH

16163028, 2023, 43, Downloaded from https://onlinelibrary.wiley.com/doi/10.1002/adfm.202303261 by Freie Universitaet Berlin, Wiley Online Library on [24/10/2023]. See the Terms and Conditions (https://onlinelibrary.wiley.com/terms-and-conditions) on Wiley Online Library for rules of use; OA articles are governed by the applicable Creative Commons License

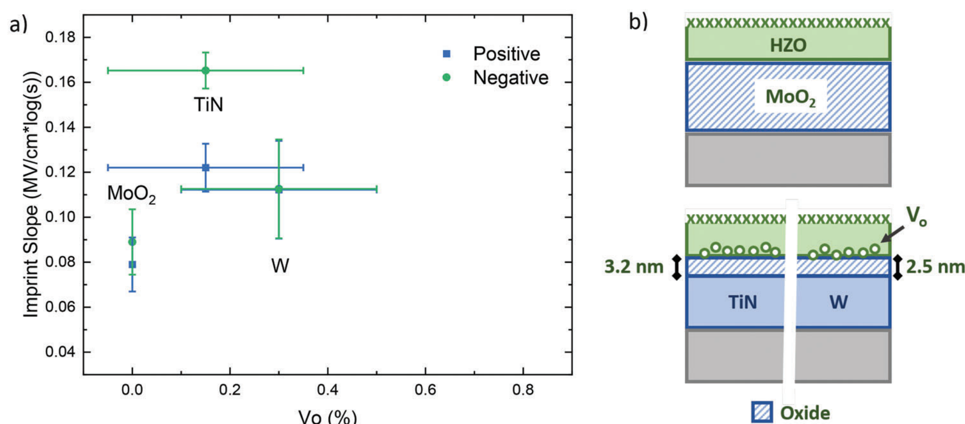

Figure 12. a) The imprint slope versus V_O concentration for HZO-based ferroelectric capacitors with a TiN TE and different BE materials. The capacitors were measured for retention after a wake-up cycling of 10^4 cycles at 3 MV cm^{-1}. b) Schematic of the two different cases were one electrode is already an oxide (MoO_2) and the other were an interface layer thickness is generated from the oxidation of the electrode (TiN/W) and V_O are generated. Interface layer thicknesses were calculated from HAXPES data as discussed in Supporting Information.

the devices did not reach breakdown within the measurement limit of 10[7] cycles, indicating increased stability, particularly for W, which presented a remarkable improvement with respect to its TE counterpart.

The retention data is shown in **Figure 12**a. The imprint slope values were similar for the different BE, with TiN presenting the highest value. Due to the low and similar V_O, it is evident how the previously discussed oxidation of the BE in the ALD chamber, before the HZO deposition, passivates the BE electrode and minimizes oxygen scavenging, improving retention in the case of non-oxide electrodes.[4,43]

From the evaluation of three different kinds of BEs, it is clear that similar trends regarding the phase composition of the HZO film can be achieved, regardless of the position. Oxide and metal electrodes can promote *m*-phase stabilization in the HZO layer due to their reduced scavenging effect compared to Ti and Nb in the form of nitride electrodes. Nevertheless, tensile stress, here suggested by a large lattice parameter ratio with respect to HZO, is also relevant for increasing the P_r. All things considered, these differences had no significant effect on endurance nor retention, highlighting the importance of the oxidation of the BE, if possible, during the ALD deposition process, which ultimately acts as a passivation step and improves the stability of the electrode during field cycling.

3. Conclusion

Asymmetrical FeCap stacks were fabricated, keeping a $Hf_{0.5}Zr_{0.5}O_2$ as the standard oxide layer and changing the bottom or top electrode while leaving the other as TiN. The electrode materials were grouped into nitrides, elemental metals, and oxides. The different electrodes allowed for an oxide interface formation analysis, which extended into defining trends in V_O concentrations in the device and crystalline phase composition. A certain amount of V_O is necessary to stabilize the ferroelectric phase but can be critical for improved field cycling behavior, endurance, and imprint during retention measurements. Since high P_r values enhance charge injection during field cycling, a compromise needs to be found between reasonable stable P_r and improved cycling endurance and retention.

From this study, it can be said that an ideal scenario would be an electrode material with a low oxygen vacancy and general defect generation potential, that is a non-reactive electrode. This is logical since defects are the source of failure during field cycling and retention. Nevertheless, the ideal electrode must also promote *o*-phase stabilization for a ferroelectric response. Due to the relationship between oxygen content and crystalline phase stabilization, a compromise is therefore necessary. Oxidizable pure metal electrodes, like W, are unfavorable due to their instability during operation, and oxide electrodes can introduce large hysteresis shifts and *m*-phase content. An idealized version of a TiN or NbN electrode, with limited oxygen scavenging behavior, possibly via a modified stoichiometry or a deliberate interface layer, is proposed from the current work. With this, the results presented in this work provide a significant contribution to the task of finding the ideal electrode configuration for ferroelectric $Hf_{0.5}Zr_{0.5}O_2$ -based next-generation memories.

4. Experimental Section

$Hf_{0.5}Zr_{0.5}O_2$ (HZO) layers were deposited in an OpAL Oxford atomic layer deposition (ALD) tool with a cycle ratio between Hf and Zr of 1:1. The precursors for hafnium and zirconium were Cp-Hf $[N(CH_3)_2]_3$, and Cp-Zr$[N(CH_3)_2]_3$, respectively. The Hf and Zr depositions were carried out at 280 °C, and ozone (O_3) was employed as the oxidant. The HZO was sandwiched between two electrodes sputtered either in an Alliance Concept CT200 sputtering tool (TiN, TiAlN, NbN, and W) or in a Bestec ultrahigh vacuum sputter cluster (W, TiN, RuO_2, and MoO_2). All electrode depositions were performed at room temperature. The RuO_2 and MoO_2 TE were deposited through a shadow mask for top contact formation, whereas all BEs and the remaining TE materials were deposited as complete films. The electrodes were deposited by sputtering from a pure metal target: for TiN, TiAlN, and NbN with 20:4 sccm Ar:N_2 ratio and 150 W, for W with 30 sccm Ar flow and 100 W power, for RuO_2, MoO_2, and IrO_2 with a process gas of a 20:5 sccm Ar:O_2 ratio and a power of about 150 W. For the purpose of GIXRD measurements, complete layers are deposited for all top electrodes. After the deposition of the top electrode, a rapid thermal anneal treatment

© 2023 The Authors. Advanced Functional Materials published by Wiley-VCH GmbH

in a N_2 atmosphere at 600 °C for 20 s was performed to crystallize the HZO films into the $Pca2_1$ polar orthorhombic phase.[31,44] In the case of TiN, TiAlN, NbN, and W, to define the final capacitor structures, Ti/Pt dots with a diameter of 200 µm and a thickness of 10 and 25 nm for Ti and Pt, respectively, were deposited via e-beam evaporation through a shadow mask. The blanket top electrode was removed using a Standard Cleaning 1 (SC1) procedure, where samples were etched in a 50:2:1 solution of water, hydrogen peroxide, and ammonia for 5 min at 50 °C.

For structural characterization, grazing incidence X-ray diffraction (GIXRD) measurements performed for this work were carried out with a Bruker D8 Discover tool with Cu-K$_\alpha$ ($\lambda = 0.154$ nm) radiation. A 2θ range from 15° to 65° was used. A simple deconvolution of the measured patterns and a Gaussian fit of the main peaks belonging to the monoclinic ($2\theta = 28.6°$ and 31.6°), the tetragonal ($2\theta = 30.8°$) and the orthorhombic ($2\theta = 30.4°$) phase was employed for phase determination. Details about the validity of this approach are discussed in the text. X-ray photoelectron spectroscopy (XPS) measurements were conducted using a monochromatic Al Kα source (1486.7 eV) and an Argus-128 (ScientaOmicron) or a Phoibos-150 (SPECS GmbH) hemispherical electron analyzers. High-resolution spectra of the Hf4*f* (from the ferroelectric film) and Ti2*p*, Nb3*d*, W4*f*, and Ru3*p* (from the TEs) were recorded using a pass energy of 20 eV, giving an overall experimental energy resolution of 0.3 eV. The take-off angle relative to the sample surface was fixed at 90°, giving a probing depth of ≈6 nm defined by ≈3λ, with λ representing the inelastic mean free path of the photo-excited electron in the material while leaving the sample. Hard X-ray photoelectron spectroscopy (HAXPES) measurements of the BE interface to HZO were carried out using two photon energies of 6 and 8 keV at the undulator BL15XU beamline,[45] part of the Japanese synchrotron SPring-8. Photoelectrons were detected by VG Scienta R4000 analyzer (ScientaOmicron). The overall energy resolution was 240 meV, verified by the Fermi cutoff of a grounded Au pad in contact with the sample. The latter was also used to define the binding energy scale. Modeling of the core level spectra was performed using CasaXPS software. Shirley backgrounds were used to subtract the inelastic secondary electron contribution. The peaks were fitted using a symmetric Voigt function, a convolution of Lorentzian (30%) and Gaussian (70%) for Hf4*f*, and asymmetric Doniach Sunjic lineshapes for metallic elements.

For electrical characterization, dynamic hysteresis and field cycling measurements were performed with a TF 3000 analyzer by aixACCT systems. Square pulses with an amplitude of 3 MV cm^{-1} and a frequency of 100 kHz were imposed during cycling. Retention and imprint measurements were performed with a Keithley 4200 electrical characterization unit. A thermo-oven was used for the baking steps during retention measurements at a temperature of 85 °C. All capacitors involved in this latter measurement underwent wake-up prior to characterization. Details on the retention measurement procedure and the extrapolation to 10 years can be found elsewhere.[46] The imprint was measured by monitoring the shift of the polarization versus voltage hysteresis loop as a function of baking time during the retention measurement for both up and down-orientated polarization states (negative and positive imprint, respectively). Impedance spectroscopy was conducted with Zurich Instruments impedance analyzer MFIA in a frequency range from 1 mHz to 5 MHz.

Supporting Information

Supporting Information is available from the Wiley Online Library or from the author.

Acknowledgements

R.A. and M.M. contributed equally to this work. P.D.L. and R.A. were funded by the German Research Foundation (DFG)—Project No. 430054035 and 433647091. This work was financially supported out of the state budget approved by the delegates of the Saxon State Parliament. N.B. and W.H. received funding from the European Union's Horizon 2020 research and innovation programme under grant agreement 780302 (3ϵFERRO). C.D. and W.H. acknowledge funding from the European Union's Horizon 2020 research and innovation programme under grant agreement 871737 (BeFerroSynaptic).

Open access funding enabled and organized by Projekt DEAL.

Conflict of Interest

The authors declare no conflict of interest.

Data Availability Statement

The data that support the findings of this study are available from the corresponding author upon reasonable request.

Keywords

capacitors, electrode materials, ferroelectricity, HfO_2, reliability, ZrO_2

Received: March 23, 2023
Revised: May 31, 2023
Published online: June 25, 2023

[1] M. Pešić, F. P. G. Fengler, L. Larcher, A. Padovani, T. Schenk, E. D. Grimley, X. Sang, J. M. LeBeau, S. Slesazeck, U. Schroeder, T. Mikolajick, *Adv. Funct. Mater.* **2016**, *26*, 4601.
[2] P. D. Lomenzo, S. Slesazeck, M. Hoffmann, T. Mikolajick, U. Schroeder, B. Max, T. Mikolajick. in *2019 19th Non-Volatile Memory Technology Symposium (NVMTS)*, IEEE, Durham, NC, USA, **2019**.
[3] R. Cao, Y. Wang, S. Zhao, Y. Yang, X. Zhao, W. Wang, X. Zhang, H. Lv, Q. Liu, M. Liu, *IEEE Electron Device Lett.* **2018**, *39*, 1207.
[4] W. Hamouda, A. Pancotti, C. Lubin, L. Tortech, C. Richter, T. Mikolajick, U. Schroeder, N. Barrett, *J. Appl. Phys.* **2020**, *127*, 064105.
[5] Y. Lee, Y. Goh, J. Hwang, D. Das, S. Jeon, *IEEE Trans. Electron Devices* **2021**, *68*, 523.
[6] M. Materano, P. D. Lomenzo, A. Kersch, M. H. Park, T. Mikolajick, U. Schroeder, *Inorg. Chem. Front.* **2021**, *8*, 2650.
[7] M. Hoffmann, U. Schroeder, T. Schenk, T. Shimizu, H. Funakubo, O. Sakata, D. Pohl, M. Drescher, C. Adelmann, R. Materlik, A. Kersch, T. Mikolajick, *J. Appl. Phys.* **2015**, *118*, 072006.
[8] P. D. Lomenzo, Q. Takmeel, C. Zhou, C. M. Fancher, E. Lambers, N. G. Rudawski, J. L. Jones, S. Moghaddam, T. Nishida, *J. Appl. Phys.* **2015**, *117*, 134105.
[9] M. Hyuk Park, H. Joon Kim, Y. Jin Kim, T. Moon, C. Seong Hwang, *Appl. Phys. Lett.* **2014**, *104*, 072901.
[10] G. Karbasian, R. dos Reis, A. K. Yadav, A. J. Tan, C. Hu, S. Salahuddin, *Appl. Phys. Lett.* **2017**, *111*, 022907.
[11] M. H. Park, H. J. Kim, Y. J. Kim, W. Lee, T. Moon, K. D. Kim, C. S. Hwang, *Appl. Phys. Lett.* **2014**, *105*, 072902.
[12] R. Cao, B. Song, D. Shang, Y. Yang, Q. Luo, S. Wu, Y. Li, Y. Wang, H. Lv, Q. Liu, M. Liu, *IEEE Electron Device Lett.* **2019**, *40*, 1744.
[13] T. Mittmann, T. Szyjka, H. A. Hsain, M. C. Istrate, P. D. Lomenzo, L. Baumgarten, M. Müller, J. L. Jones, L. Pintilie, T. Mikolajick, U. Schroeder, *Phys. Status Solidi RRL 15*, 2100012.
[14] M. H. Park, H. J. Kim, Y. J. Kim, W. Jeon, T. Moon, C. S. Hwang, *Phys. Status Solidi RRL* **2014**, *8*, 532.
[15] Y. Goh, S. H. Cho, S.-H. K. Park, S. Jeon, *Nanoscale* **2020**, *12*, 9024.
[16] Y. Goh, S. H. Cho, S.-H. K. Park, S. Jeon, *IEEE Trans. Electron Devices* **2020**, *67*, 3431.
[17] M. Müller, P. Lömker, P. Rosenberger, M. Hussein Hamed, D. N. Mueller, R. A. Heinen, T. Szyjka, L. Baumgarten, *J. Vac. Sci. Technol., A* **2022**, *40*, 013215.

© 2023 The Authors. Advanced Functional Materials published by Wiley-VCH GmbH

16163028, 2023, 43, Downloaded from https://onlinelibrary.wiley.com/doi/10.1002/adfm.202303261 by Freie Universitaet Berlin, Wiley Online Library on [24/10/2023]. See the Terms and Conditions (https://onlinelibrary.wiley.com/terms-and-conditions) on Wiley Online Library for rules of use; OA articles are governed by the applicable Creative Commons License

[18] M. Hoffmann, U. Schroeder, C. Künneth, A. Kersch, S. Starschich, U. Böttger, T. Mikolajick, *Nano Energy* **2015**, *18*, 154.
[19] G. Holzlechner, D. Kastner, C. Slouka, H. Hutter, J. Fleig, *Solid State Ionics* **2014**, *262*, 625.
[20] H. Fujisawa, S. Hyodo, K. Jitsui, M. Shimizu, H. Niu, H. Okino, T. Shiosaki, *Integr. Ferroelectr.* **1998**, *21*, 107.
[21] K. Shubhakar, K. L. Pey, N. Raghavan, S. S. Kushvaha, M. Bosman, Z. Wang, S. J. O'Shea, *Microelectron. Eng.* **2013**, *109*, 364.
[22] A. Chouprik, E. Kondratyuk, V. Mikheev, Y. Matveyev, M. Spiridonov, A. Chernikova, M. G. Kozodaev, A. M. Markeev, A. Zenkevich, D. Negrov, *Acta Mater.* **2021**, *204*, 116515.
[23] Y. Lee, H. Alex Hsain, S. S. Fields, S. T. Jaszewski, M. D. Horgan, P. G. Edgington, J. F. Ihlefeld, G. N. Parsons, J. L. Jones, *Appl. Phys. Lett.* **2021**, *118*, 012903.
[24] F. P. G. Fengler, M. Pešić, S. Starschich, T. Schneller, C. Künneth, U. Böttger, H. Mulaosmanovic, T. Schenk, M. H. Park, R. Nigon, P. Muralt, T. Mikolajick, U. Schroeder, *Adv. Electron. Mater.* **2017**, *3*, 1600505.
[25] R. Alcala, P. D. Lomenzo, T. Mittman, B. Xu, R. Guido, S. Lancaster, P. Vishnumurthy, L. Grenouillet, S. Martin, J. Coignus, T. Mikolajick, U. Schroeder, presented at *IEDM*, xx, San Francisco, CA, USA December **2022**.
[26] T. Schenk, M. Hoffmann, M. Pešić, M. H. Park, C. Richter, U. Schroeder, T. Mikolajick, *Phys. Rev. Appl.* **2018**, *10*, 064004.
[27] F. Mehmood, R. Alcala, P. Vishnumurthy, B. Xu, R. Sachdeva, T. Mikolajick, U. Schroeder, *Adv. Mater. Interfaces* **2023**.
[28] D. R. Islamov, T. M. Zalyalov, **2022**, https://doi.org/10.48550/ARXIV.2212.10858.
[29] B. Max, M. Pešić, S. Slesazeck, T. Mikolajick, *J. Appl. Phys.* **2018**, *123*, 134102.
[30] J. W. McPherson, *Microelectron. Reliab.* **2012**, *52*, 1753.
[31] M. Materano, T. Mittmann, P. D. Lomenzo, C. Zhou, J. L. Jones, M. Falkowski, A. Kersch, T. Mikolajick, U. Schroeder, *ACS Appl. Electron. Mater.* **2020**, *2*, 3618.
[32] T. Mittmann, M. Materano, P. D. Lomenzo, M. H. Park, I. Stolichnov, M. Cavalieri, C. Zhou, C. Chung, J. L. Jones, T. Szyjka, M. Müller, A. Kersch, T. Mikolajick, U. Schroeder, *Adv. Mater. Interfaces* **2019**, *6*, 1900042.
[33] W. Shen, R. Dittmann, U. Breuer, R. Waser, *Appl. Phys. Lett.* **2008**, *93*, 222102.
[34] G. González-Cordero, F. Jiménez-Molinos, J. B. Roldán, M. B. González, F. Campabadal, *Meas. Phenom.* **2017**, *35*, 01A110.
[35] P. S. Lysaght, in *AIP Conference Proceedings*, AIP, Richardson, Texas (USA) **2005**.
[36] R. Alcala, M. Materano, P. D. Lomenzo, L. Grenouillet, T. Francois, J. Coignus, N. Vaxelaire, C. Carabasse, S. Chevalliez, F. Andrieu, T. Mikolajick, U. Schroeder, *IEEE J. Electron Devices Soc.* **2022**, *10*, 907.
[37] A. A. Demkov, L. R. C. Fonseca, E. Verret, J. Tomfohr, O. F. Sankey, *Phys. Rev. B* **2005**, *71*, 195306.
[38] Y. Matveyev, V. Mikheev, D. Negrov, S. Zarubin, A. Kumar, E. D. Grimley, J. M. LeBeau, A. Gloskovskii, E. Y. Tsymbal, A. Zenkevich, *Nanoscale* **2019**, *11*, 19814.
[39] T. Song, H. Tan, A.-C. Robert, S. Estandia, J. Gázquez, F. Sánchez, I. Fina, *Appl. Mater. Today* **2022**, *29*, 101621.
[40] I. Levin, **2020**, https://doi.org/10.18434/M32147.
[41] Database, International Centre for Diffraction Data, **2022**.
[42] T. Szyjka, L. Baumgarten, T. Mittmann, Y. Matveyev, C. Schlueter, T. Mikolajick, U. Schroeder, M. Müller, *Physica RRL* **2021**, *15*, 2100027.
[43] L. Baumgarten, T. Szyjka, T. Mittmann, M. Materano, Y. Matveyev, C. Schlueter, T. Mikolajick, U. Schroeder, M. Müller, *Appl. Phys. Lett.* **2021**, *118*, 032903.
[44] X. Sang, E. D. Grimley, T. Schenk, U. Schroeder, J. M. LeBeau, *Appl. Phys. Lett.* **2015**, *106*, 162905.
[45] S. Ueda, Y. Katsuya, M. Tanaka, H. Yoshikawa, Y. Yamashita, S. Ishimaru, Y. Matsushita, K. Kobayashi, *AIP Conf. Proc.* **2010**, *1234*, 403.
[46] S. Mueller, J. Muller, U. Schroeder, T. Mikolajick, *IEEE Trans. Device Mater. Reliab.* **2013**, *13*, 93.

© 2023 The Authors. Advanced Functional Materials published by Wiley-VCH GmbH

16163028, 2023, 43, Downloaded from https://onlinelibrary.wiley.com/doi/10.1002/adfm.202303261 by Freie Universitaet Berlin, Wiley Online Library on [24/10/2023]. See the Terms and Conditions (https://onlinelibrary.wiley.com/terms-and-conditions) on Wiley Online Library for rules of use; OA articles are governed by the applicable Creative Commons License